FLORE
Repository istituzionale dell'Università degli Studi di Firenze

Seismic anisotropy reveals a dynamic link between adjacent magmatic segments prior to dyke intrusion

Questa è la Versione finale referata (Post print/Accepted manuscript) della seguente pubblicazione:

Original Citation:

Seismic anisotropy reveals a dynamic link between adjacent magmatic segments prior to dyke intrusion / Illsley-Kemp, F., Greenfield, T., Keir, D.. - In: JOURNAL OF GEOPHYSICAL RESEARCH. SOLID EARTH. - ISSN 2169-9356. - ELETTRONICO. - 123:(2018), pp. 1-17. [10.1029/2018JB016420]

Availability:

This version is available at: 2158/1144379 since: 2020-10-29T10:02:57Z

Published version:

DOI: 10.1029/2018JB016420

Terms of use:

Open Access

La pubblicazione è resa disponibile sotto le norme e i termini della licenza di deposito, secondo quanto stabilito dalla Policy per l'accesso aperto dell'Università degli Studi di Firenze (https://www.sba.unifi.it/upload/policy-oa-2016-1.pdf)

Publisher copyright claim:

(Article begins on next page)

25 November 2024

Journal of Geophysical Research: Solid Earth

RESEARCH ARTICLE
10.1029/2018JB016420

Seismic Anisotropy Reveals a Dynamic Link Between Adjacent Magmatic Segments Prior to Dyke Intrusion

Finnigan Illsley-Kemp[1,2], **Tim Greenfield**[1], **and Derek Keir**[1,3]

[1]Ocean and Earth Science, University of Southampton, Southampton, UK, [2]School of Geography, Environment and Earth Sciences, Victoria University of Wellington, Wellington, New Zealand, [3]Dipartimento di Scienze della Terra, Universita degli Studi di Firenze, Florence, Italy

Key Points:
- We detail time-varying, crustal seismic anisotropy around a dyke intrusion in the Afar depression
- The magnitude of seismic anisotropy is shown to increase during the dyke intrusion, suggesting pressurization of the hydrothermal system
- Change in anisotropy prior to dyke intrusion reveals inflation of magma chamber in adjacent rift segment, suggesting lateral flow of magma

Supporting Information:
- Supporting Information S1
- Data Set S1
- Data Set S2
- Data Set S3
- Data Set S4
- Data Set S5
- Data Set S6
- Data Set S7

Correspondence to:
F. Illsley-Kemp,
finnigan.illsleykemp@vuw.ac.nz

Citation:
Illsley-Kemp, F., Greenfield, T., & Keir, D. (2018). Seismic anisotropy reveals a dynamic link between adjacent magmatic segments prior to dyke intrusion. *Journal of Geophysical Research: Solid Earth*, *123*. https://doi.org/10.1029/2018JB016420

Received 19 JUL 2018
Accepted 21 OCT 2018
Accepted article online 24 OCT 2018

©2018. The Authors.
This is an open access article under the terms of the Creative Commons Attribution License, which permits use, distribution and reproduction in any medium, provided the original work is properly cited.

Abstract Seismic anisotropy has increasingly been proposed as a tool in the monitoring of magmatic systems and potential forecasting of volcanic eruptions. We present a detailed study of how seismic anisotropy evolves in an active magmatic rift segment before, during, and after a dyke intrusion in the Afar depression, Ethiopia. Results show that seismic anisotropy prior to the dyke intrusion is controlled by a complex and deforming magma plumbing system beneath the adjacent Dabbahu and Manda-Hararo magmatic segments. Approximately eight days prior to the dyke intrusion in the Dabbahu segment, the pattern of anisotropy, coupled with lower crustal seismicity, is best explained by the inflation of a lower crustal magma reservoir in the Manda-Hararo segment. This is the only clearly observed precursory change in seismic anisotropy. During the dyke intrusion, the magnitude of seismic anisotropy increases twofold, before rapidly returning to predyke values once the intrusion has ended. Combining our observations with models of magmatically induced crustal stress, we propose that when the deep magma reservoir beneath the Dabbahu segment becomes overpressured, inflation is triggered in the magma reservoir of the neighboring Manda-Hararo segment. This provides strong evidence for a hydraulic link between the deep magma systems of the neighboring rift segments and that magma reservoirs beneath the Dabbahu segment can be fed by the lateral flow of magma from an adjacent segment. Our results demonstrate that seismic anisotropy has the potential to be a powerful tool for monitoring deformation in the magma plumbing systems of active volcanoes.

1. Introduction

1.1. Seismic Anisotropy in the Crust

Seismic anisotropy is an intrinsic property of the Earth's crust and is observed in almost all geological and tectonic settings (e.g., Illsley-Kemp, Savage, et al., 2017; Johnson et al., 2011; Li & Peng, 2017; Menke et al., 1994). Numerous studies have suggested that seismic anisotropy is caused by structural features such as faults (e.g., Boness & Zoback, 2006; Li et al., 2014; Menke et al., 1994; Zinke & Zoback, 2000), and aligned melt pockets (e.g., Bastow et al., 2010; Dunn et al., 2005; Keir et al., 2005, 2011), where the polarization direction is parallel to the trend of structural features. It has also been increasingly observed that seismic anisotropy in the crust can be controlled by aligned, fluid-filled microcracks (Crampin & Peacock, 2008, and references therein.). Microcracks exist between grains and can be assumed to have a simple, penny-shaped geometry (Crampin, 1994, 1999). It is thought that these microcracks are randomly oriented in the crust and do not intrinsically induce seismic anisotropy. However, when a horizontal stress is applied to the crust, microcracks will selectively open to align with the direction of maximum horizontal compressive stress. These aligned, fluid-filled microcracks will induce seismic anisotropy through a mechanism described as extensive dilatancy anisotropy (EDA; Crampin, 1984, 1987). The variation in orientations of individual, open microcracks can vary by ~30–40° (Crampin & Zatsepin, 1997). However, the wavelength of seismic waves is much larger than the dimensions of the microcracks; hence, the average crack orientation is sampled by seismological techniques. The magnitude of seismic anisotropy (i.e., the delay time between shear waves) has been shown to be controlled by the aspect ratio (ratio between width and length) of the microcracks (Crampin, 1999). The microcrack's aspect ratio correlates with the horizontal stress; thus, the magnitude of seismic anisotropy is directly related to the magnitude of maximum horizontal stress. Therefore, through the theory of EDA, seismic anisotropy can be used to directly measure the orientation and magnitude of the horizontal stress field in the crust.

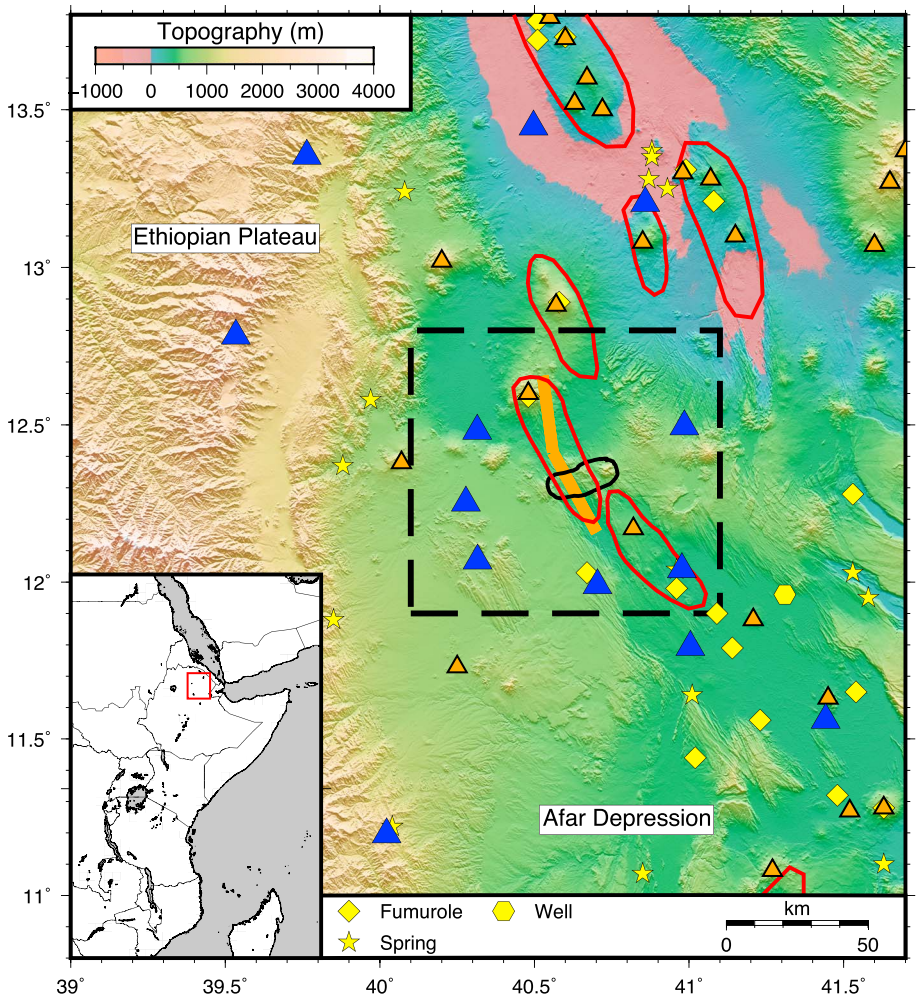

Figure 1. Topographic map of the northern Afar depression. Seismic network (blue triangles) deployed from 11 October 2009 to 18 November 2010. The orange triangles denote active volcanic centers. The red segments denote the Quaternary magmatic segments. The location of the 2005 dyke intrusion within the Dabbahu segment is denoted in orange (Wright et al., 2006). Figure 2 outline shown by dashed black box. Hydrothermal features taken from Keir et al. (2009). Inset shows the location of the study region in East Africa.

1.2. Temporally Varying Anisotropy

Many studies have observed that crustal seismic anisotropy can vary temporally in response to geological phenomena in which changes to the orientation and magnitude of the stress field are expected. Shear-wave delay time has been observed to increase prior to earthquakes (Peacock et al., 1988; Volti & Crampin, 2003), with the suggestion that as stress builds, the microcrack aspect ratios in a rock volume increase, causing an increase in shear-wave delay time. Once the stress is released by the earthquake, the microcracks and shear-wave delay time instantaneously return to their previous state. This observation has led authors to suggest that seismic anisotropy may act as a tool for earthquake forecasting. However, the ability of seismic anisotropy to forecast large earthquakes is not universally accepted (Aster et al., 1990; Crampin et al., 1991).

Building on the premise that temporally varying seismic anisotropy can monitor changes in crustal stresses, several studies have investigated seismic anisotropy in regions of volcanic unrest. Both the orientation and magnitude of seismic anisotropy have been reported to respond to volcanic activity at, among others, Mt. Ruapehu, New Zealand (Gerst & Savage, 2004; Miller & Savage, 2001); Mt. Etna, Italy (Bianco et al., 2006); Soufriére Hills, Montserrat (Roman et al., 2011); and Piton de la Fournaise, La Rèunion (Savage et al., 2015). These studies have typically found that the orientation of seismic anisotropy changes in

response to volcanic activity. Seismic anisotropy has also been observed to respond to changes in fluid pressure in the Krafla geothermal reservoir, Iceland (Tang et al., 2005). However, due to the relative infrequency of subaerial dyke intrusions, our understanding of how seismic anisotropy and crustal stress evolves during these events is limited. Dyke intrusions are an important process in continental rifting (e.g., Wright et al., 2012) and seafloor spreading (e.g., Ahmed et al., 2016; Tan et al., 2016); it is therefore vital that we understand the dynamic evolution of crustal stress during these rifting events.

1.3. The Dabbahu Rifting Sequence

An ideal locale to study how crustal anisotropy responds to a dyke intrusion is the Dabbahu rift segment, Ethiopia. The Dabbahu rift segment is at the southern end of the Red Sea rift system and forms part of the subaerial Afar depression (Figure 1). The Afar depression lies at the triple junction of the Red Sea, Gulf of Aden, and Main Ethiopian rifts (McKenzie & Davies, 1970). Rifting in Afar initiated ~29–31 Ma with extension initially focused on large border faults (Ayalew et al., 2006; Wolfenden et al., 2005). Between 25 and 20 Ma, the majority of extension in Afar is thought to have migrated away from the border faults (Hayward & Ebinger, 1996; Wolfenden et al., 2005) and is now focused at axial magmatic segments. These magmatic segments are the locus for the majority of present-day seismicity and magmatism (Belachew et al., 2011; Illsley-Kemp et al., 2018; Wright et al., 2006). The ~60-km-long, ~20-km-wide Dabbahu segment consists of a central valley bound by normal faults, which trend NNW-SSE in the north and NW-SE in the south (Medynski et al., 2013). The center of the segment is characterized by the axial Ado'Ale Volcanic Complex (AVC), with a large collapse structure (Medynski et al., 2013). Dabbahu stratovolcano is at the northern end of the segment (Field et al., 2012). Between 20 September 2005 and 4 October 2005, the entire segment was intruded by an 80-km-long, 10-km-deep, and 8-m-wide dyke (Ayele et al., 2007; Wright et al., 2006). This initiated an ~5-year-long rifting sequence, which involved the intrusion of a further 13 dykes (Barnie et al., 2015; Belachew et al., 2011; Hamling et al., 2009). Each dyke typically propagated north or south from the AVC in a pattern that is thought to have been controlled by preexisting crustal structures and the unclamping of stresses by preceding dyke intrusions (Grandin et al., 2010; Hamling et al., 2009, 2010). Ground deformation between dyke intrusions has been modeled to reveal that the dykes are sourced from a composite dyke-sill magma chamber beneath the center of the rift segment, which inflates at a near-constant rate during the rifting sequence (Grandin et al., 2010). The ground deformation signal also revealed deep-crustal magma reservoirs beneath the Dabbahu segment and adjacent Manda Hararo segment. The deep magma reservoir beneath the Dabbahu segment (W3) is modeled at 25-km depth and inflates at a near-constant rate of +0.13 km^3/year between 2005 and 2009, when observations end. Similarly, the magma reservoir beneath the Manda Hararo segment (*H*) is modeled at 17-km depth; however, this reservoir is observed to deflate at a constant rate of −0.13 km^3/year, complementary to the inflation at depth beneath the Dabbahu segment (Grandin, Socquet, Doin, et al., 2010).

The rifting sequence finished with an intrusive event in May 2010, a dyke propagated to the north and south of the AVC. The sequence of events during this dyke intrusion has been well established by Barnie et al. (2015), using a combination of seismicity, interferometric synthetic aperture radar, satellite thermal data, ultraviolet SO_2 retrievals, and light detection and ranging imagery. The intrusion initiated at 20 May, 18:09 when seismic activity revealed the ascent of magma at the AVC, seismicity then propagated both north and south to maximum extents of 8 and 10 km, respectively. Barnie et al. (2015) suggest that this seismicity tracked the propagating tips of the dyke and that the north and south propagation finished at 21 May, 00:00 and 08:00, respectively. Cessation of dyke propagation to the north is coincident with a fissure eruption that began between 00:57 and 01:12 21 May, with effusion rates peaking at 02:27 and stopping entirely by 06:27. The total erupted volume is calculated to be 0.23×10^6 m^3 (Barnie et al., 2015). The dynamic sequence of events during this dyke intrusion is well understood, and the intrusion was monitored by an excellent seismic network; it thus provides an ideal opportunity to study how crustal seismic anisotropy responds to a dyke intrusion.

The Dabbahu rifting episode consisted of 13 dyke intrusions over a 5-year period (Barnie et al., 2015; Belachew et al., 2011; Hamling et al., 2009). The stress field surrounding the Dabbahu segment will have been influenced by each of these intrusions and thus can be expected to be complex in nature. Illsley-Kemp, Savage, et al. (2017) conducted a study of seismic anisotropy across Northern Afar between 2011 and 2013 and found that anisotropy orientations in the Dabbahu region did not agree with a previous study of Keir et al. (2011). It was suggested that the data of Keir et al. (2011) were influenced by the Dabbahu rifting

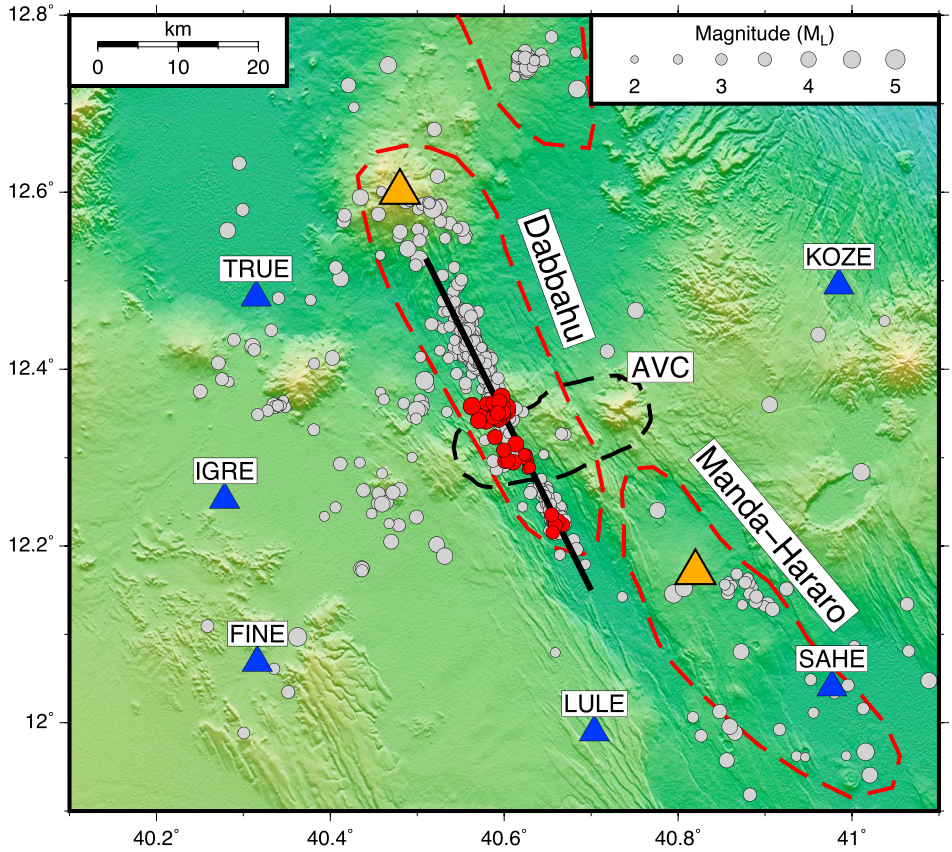

Figure 2. Seismic network (blue triangles) deployed in Afar from 11 October 2009 to 18 November 2010. Earthquakes shown by grey circles; dyke-induced earthquakes are red circles. The black line denotes profile for Figure 3. The Dabbahu and Manda-Hararo magmatic segments are labeled. The orange triangles denote the Dabbahu and Manda-Hararo volcanoes. The Ado'Ale volcanic segment (AVC) is shown with a dashed black line.

sequence and that this caused the disagreement in anisotropy orientations. In this study we aim to develop on the work of Illsley-Kemp, Savage, et al. (2017) and study the temporal evolution of crustal seismic anisotropy in the Dabbahu rift segment.

2. Data and Methods

2.1. Seismic Data

We used continuous seismic data from a network of 13 Güralp broadband seismometers deployed between October 2009 and November 2010 (Figure 2). Earthquakes were detected and located automatically using coalescence microseismic mapping (Drew et al., 2013). This generates a characteristic function for each recorded channel by calculating a ratio between the average amplitude in a short window (0.3 s) and the amplitude in a longer window (5 s). Peaks in the characteristic function are fitted with Gaussian envelopes and then migrated through a 1-D velocity model (from Belachew et al., 2011). Maxima in the coalescence function record the temporal and spatial coordinates of detected earthquakes. To avoid artifacts, we only output those earthquakes with signal-to-noise ratios greater than 2. We searched over a defined region in Afar and the final catalog contains 1,190 individual earthquakes. Local magnitudes are then calculated using a region-specific magnitude scale (Illsley-Kemp, Keir, et al., 2017; Figure 2).

2.2. Seismic Anisotropy

Automatic *S*-picks from coalescence microseismic mapping are generally slightly later than the actual onset (Greenfield et al., 2016); we therefore manually picked 4,650 *S* wave arrivals for the entire catalog at all 13 seismic stations. We then applied the Multiple Filter Automatic Splitting Technique Version 2.2

Table 1
Seismic Anisotropy Results for Individual Stations (Figure 4)

Station	Num. Meas.	Predyke Φ (°)	Codyke Φ (°)	Postdyke Φ (°)	Predyke δt (10^{-4} s/km)	Codyke δt (10^{-4} s/km)	Postdyke δt (10^{-4} s/km)
FINE	176	50 ± 8	46 ± 17	36 ± 17	36 ± 2	46 ± 2	36 ± 1
IGRE	280	88 ± 1	74 ± 3	85 ± 2	28 ± 1	39 ± 1	30 ± 1
KOZE	24	79 ± 24	54 ± 27	52 ± 21	16 ± 1	76 ± 3	30 ± 1
LULE	49	−45 ± 11	−23 ± 4	−32 ± 2	44 ± 1	58 ± 1	37 ± 1
SAHE	100	77 ± 4	−49 ± 9	70 ± 5	24 ± 1	114 ± 15	50 ± 8
TRUE	39	23 ± 6	−40 ± 5	11 ± 10	25 ± 1	117 ± 2	27 ± 1

Note. Axial mean anisotropy orientation (Φ) given in degrees clockwise from north. Average delay time at each station (δt) given in seconds per kilometer. Errors are given by one standard deviation from the mean.

(MFAST; Savage et al., 2010). MFAST is based on the method of Silver and Chan (1991) and minimizes the covariance matrix eigenvalue of the horizontal particle motion by searching over a range of fast direction (φ) and delay times (δt). MFAST then develops the method of Teanby et al. (2004) by trialing a set of 14 filters over the *S* wave pick and determines the three most effective filters by analyzing the signal-to-noise ratio. These filters are then used with the Silver and Chan (1991) method to measure shear-wave splitting over multiple windows. The reliability of these measurements is then assessed by cluster analysis, with unreliable results being discarded. Further, MFAST rejects measurements, which have an unclear linearity by assessing the smallest and largest eigenvalues. This rigorous quality analysis allows us to interpret shear-wave splitting results with a high degree of confidence. Errors for individual measurements are directly calculated from the contours of the shear-wave splitting grid search (Silver & Chan, 1991). Average values for both fast direction (φ) and delay times (δt) are calculated over the three time periods of interest with errors given by the standard deviation of values within the specified time period (Table 1). In order to consider errors in fast direction, we calculate the von Mises distribution (Mardia & Jupp, 2000) of fast directions in each time period. This is characterized by a mean fast direction (Φ) and a concentration parameter (κ). The concentration parameter gives an indication of the distribution of fast directions, with a value of 0 indicating a random distribution, and is used to calculate standard errors in fast direction. We calculate high concentration parameters for distinct time periods at stations of interest (Table S1), suggesting a statistically robust, preferred fast-orientation.

We use the TauP toolkit (Crotwell et al., 1999) to determine earthquake raypath incidence angles at the surface in order to limit raypaths to the shear-wave window. The shear-wave window is the vertical cone beneath the seismic station bound by $\sin^{-1}(V_S/V_P)$. This removes any potential contamination from phase conversions at the surface (Booth & Crampin, 1985).

As we are interested in the evolution of seismic anisotropy in response to the May 2010 dyke intrusion, we limit our study to consider only anisotropy results from earthquakes that occur within the Dabbahu segment region (Figure 4). This allows us to consider temporal changes in seismic anisotropy by minimizing the influence of variable path effects.

3. Results

3.1. Seismicity

Out of our total catalog we use 599 individual earthquakes in the Dabbahu region with magnitudes ranging from 2.4 to 4.9 M_L and the catalog is complete above 3.2 M_L (Woessner & Wiemer, 2005; Figure 2). The seismicity of the May 2010 dyke intrusion is well described by Barnie et al. (2015). Our longer seismic catalog reveals that the rupture area of the dyke is seismically quiet for all periods before and after the dyke intrusion and the vast majority of seismicity in the Dabbahu segment is focused north of the segment center in the region ruptured by previous dyke intrusions (Figure 3). We use the study of Barnie et al. (2015) to define the beginning and end of dyke propagation.

3.2. Seismic Anisotropy

At stations near the dyke intrusion, we record a total of 674 measurements of seismic anisotropy that are classed as A or B by MFAST (Table 1). We see no response of the seismic anisotropy to the May 2010 dyke

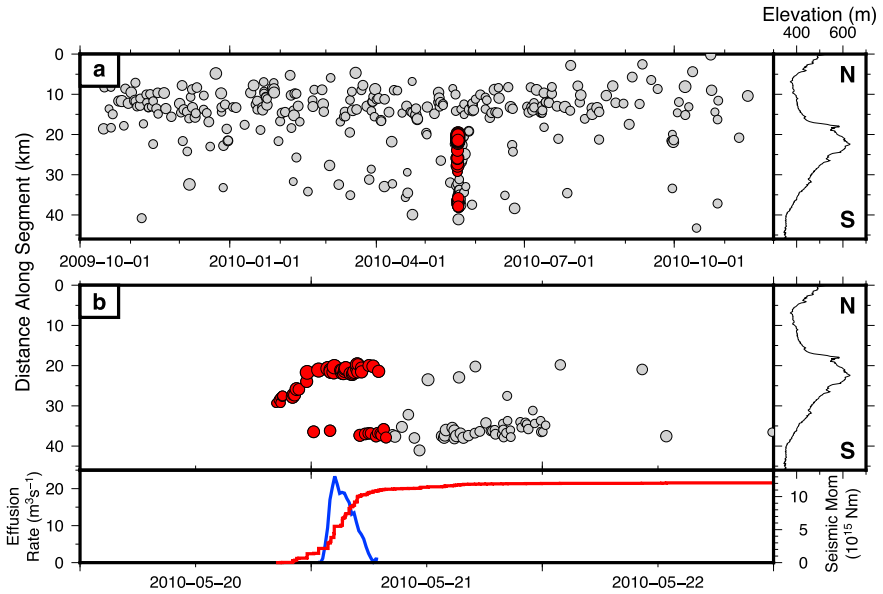

Figure 3. (a) Along segment seismicity through time (Figure 2). The May 2010 dyke rupture area is seismically quiet for all nonintrusive time periods. During these times, seismicity is focused in the north of the Dabbahu segment. (b) The two separate dyke intrusions (red) to the north and south are clearly visible. Seismicity immediately after the southern dyke intrusion is interpreted as a response to the dyke intrusion and not the direct result of dyke propagation (Barnie et al., 2015) effusion rate (blue) derived from extracted SEVIRI band 3 (1.6 μm) radiance marks the timing and volume of the fissure eruption (Barnie et al., 2015). Cumulative seismic moment release is shown in red.

intrusion at any station that is further than 50 km from the dyke. We will therefore exclusively consider the seismic anisotropy results at those stations nearby the dyke intrusion (Figure 2). Seismic anisotropy is accrued along the raypath; therefore, a significant change in earthquake location can result in a change in seismic anisotropy measurements due to the different volumes that are being sampled. This could be mistakenly interpreted as a temporal change in seismic anisotropy within the volume. In order to ensure that any temporal variations we observe are not originating from a change in the volume being sampled, we examine temporal variations in the raypath properties; back azimuth (°), source depth (km), and incidence angle at the seismometer (°; Figures S4–S6). We find that there is very little variation in raypath properties through time; thus, any observed variations in seismic anisotropy can be attributed to changes within the same sampled volume.

By averaging the observed delay time along the length of the raypath we find that prior to the dyke intrusion the average anisotropy recorded at the proximal stations is 38×10^{-4} s/km (Table 1). Anisotropy orientations (Figure 4a) are generally consistent with previous studies of the region (Illsley-Kemp, Savage, et al., 2017; Keir et al., 2011) and show no clear coherent orientation between stations. Individual stations show little internal variation, with the exception of KOZE, which has two distinct populations of anisotropy orientations.

At every station, we observe an increase in average delay time (δt) during the dyke intrusion by an average ratio of 2.03 (Table 1). We also observe a change in the orientation of seismic anisotropy during the dyke intrusion at most stations (Figure 4b and Table 1); this is most pronounced at stations SAHE, FINE, TRUE, and IGRE (Figures 4 and 5). FINE shows more scatter in anisotropy orientation than the other stations (Figure 5); however, there is a distinct population of orientation measurements at ~50° before and after the dyke intrusion. During the dyke intrusion there is a range of orientation measurements, yet there appears to be two populations of orientations at approximately 30 and −80° (Figure 6). The increase in delay time at FINE appears to occur ~24 hr before the dyke intrusion. IGRE changes from a predyke orientation of 88° to a codyke orientation of 74°. This change appears to occur simultaneously with the initiation of the dyke intrusion and is coincident with an increase in delay time (Figure 6). The orientation of anisotropy at TRUE changes from 19° predyke to −39° during the dyke intrusion. The delay time also increases markedly during the dyke intrusion (Figure 6). Due to a lack of high-quality measurements at TRUE between 14 May 2010 and the

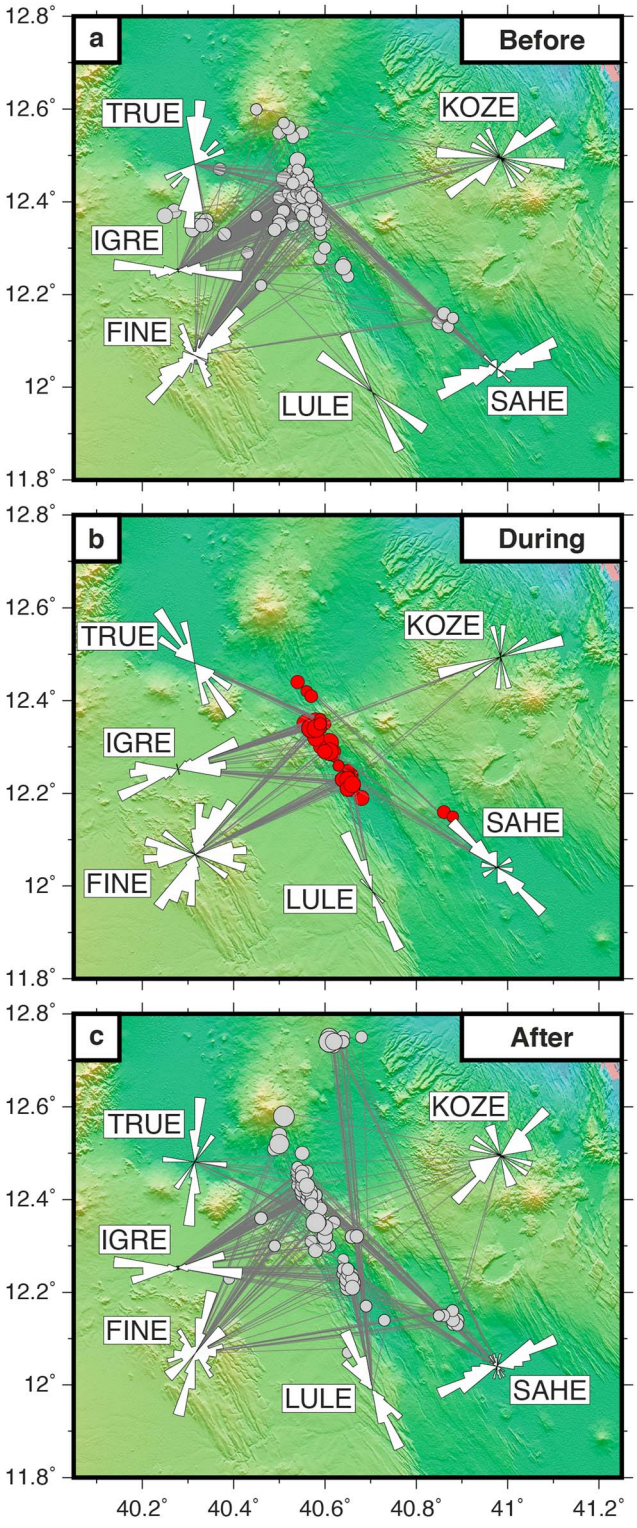

Figure 4. Rose diagrams showing seismic anisotropy orientations (φ). (a) Seismic anisotropy before the dyke intrusion (00:00:00, 11 October 2009, to 18:09:00, 20 May 2010). (b) Seismic anisotropy during the dyke intrusion (18:09:00, 20 May 2010, to 16:00:00, 21 May 2010). (c) Seismic anisotropy after the dyke intrusion (16:00:00, 21 May 2010, to 23:59:59, 18 November 2010).

initiation of the dyke intrusion, it is not possible to identify at which point the change in anisotropy occurred. SAHE changes from a predyke orientation of 79° to an orientation of −54° during the dyke intrusion. The orientation change at SAHE occurs on 11 May 2010 and is coincident with an increase in delay time (Figure 6). This change in seismic anisotropy happens ~8 days prior to the dyke intrusion.

Once the dyke has ceased propagating, both the anisotropy orientation and delay times return almost immediately to values that are very similar to the predyke measurements (Table 1 and Figure 4c). This change does not occur at the exact time at which the dyke stops propagating (08:00:00, 21 May 2010), at SAHE and FINE the anisotropy changes ~8 hr after dyke propagation (Figure 6). At approximately 1 July 2010, the anisotropy at SAHE shows a change that is similar to that observed during the May 2010 dyke intrusion. This change in anisotropy is not clearly linked to any increase in seismicity in the Dabbahu segment.

4. Discussion

4.1. Predyke Anisotropy

Previous studies of crustal seismic anisotropy in the East African rift have generally found that the anisotropy aligns with the regional stress field and/or with rift-aligned structures (Illsley-Kemp, Savage, et al., 2017; Keir et al., 2005, 2011). If a similar mechanism was controlling the anisotropy in the Dabbahu rift segment, one would expect the anisotropy to align NNW-SSE, parallel to the Red Sea rift. Our study has shown that anisotropy in this region (before and after the dyke intrusion) is not aligned with the rift and shows a large amount of local variation (Figures 4a and 4c). Surface faulting in the Dabbahu region shows a predominance of NNW-SSE aligned structures (Manighetti et al., 2001; Medynski et al., 2016); this may explain the predyke anisotropy orientation at LULE and TRUE, but the other stations display orientations that are highly oblique to these faults. Therefore, we can rule out structure-controlled anisotropy as the dominant mechanism for inducing seismic anisotropy. Similarly, if the anisotropy was controlled by the large-scale tectonic forces of the Red Sea rift, it would also align NNW-SSE, perpendicular to the extension direction. This can therefore also be discounted on a similar basis.

In regions of magmatic activity, it has been observed that local seismic anisotropy can be controlled by volume changes in the magmatic plumbing system (Gerst & Savage, 2004; Roman et al., 2011; Savage et al., 2015). Ground deformation measurements between the Dabbahu dyke intrusions can be modeled by several inflating and deflating magmatic sources (Grandin, Socquet, Doin, et al., 2010; Temtime et al., 2018). Two magma bodies beneath Dabbahu volcano, at the northern end of the rift segment (Figure 2), show a large initial response to the initial 2005 dyke intrusion but then stop deforming by mid-2006 and 2008, respectively. Additionally, five other magmatic bodies are modeled to deform at a near-constant rate from mid-2006 to mid-2009 when the interferometric synthetic aperture radar data ends. Included in this model are two deep magma reservoirs, Wal'lis (W1) and Hararo (H), which are beneath the Dabbahu and Manda-Hararo segments, respectively (Figure 7). If we assume that these bodies continued to deform at a constant rate through to 2010, we are able to model the effect that they have on the horizontal stress field in the

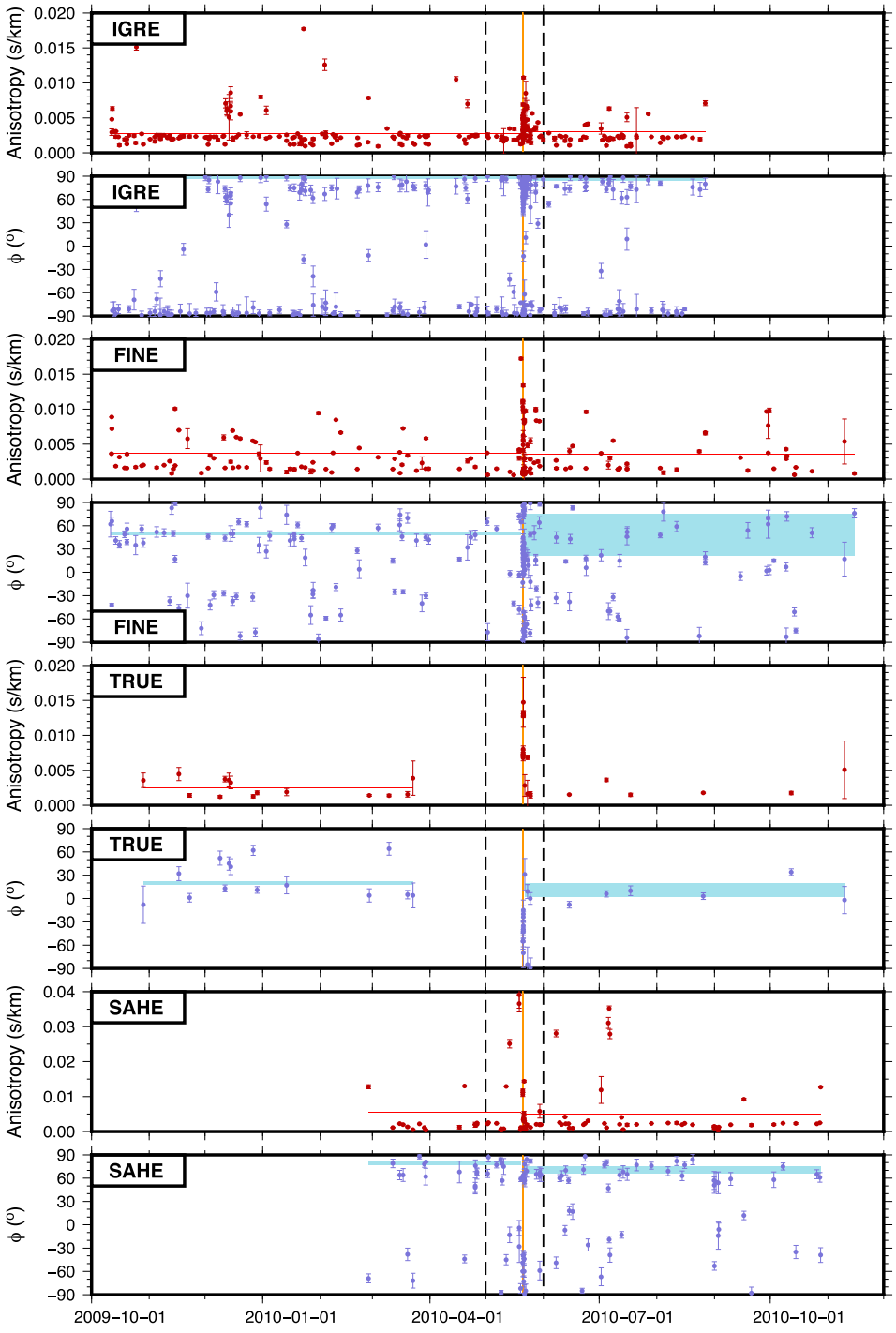

Figure 5. Seismic anisotropy through time at IGRE, FINE, TRUE, and SAHE. The colored background boxes indicate the mean value ± error, before and after the dyke intrusion. The dashed box indicates the time window for Figure 6. The orange box indicates time at which the dyke was propagating. Note the different *Y* axis for anisotropy (s/km) at SAHE.

Dabbahu region. We use the Coulomb 3.3 package (Lin & Stein, 2004; Toda et al., 2005) to model the deforming magma bodies and to extract the orientation of the modeled maximum horizontal stress at the surface. By using the EDA principal that seismic anisotropy will align with the direction of maximum horizontal stress we can directly compare our measurements of seismic anisotropy with the modeled stress field (Figure 7). The modeled SH_{max} orientation is shown to vary over relatively short

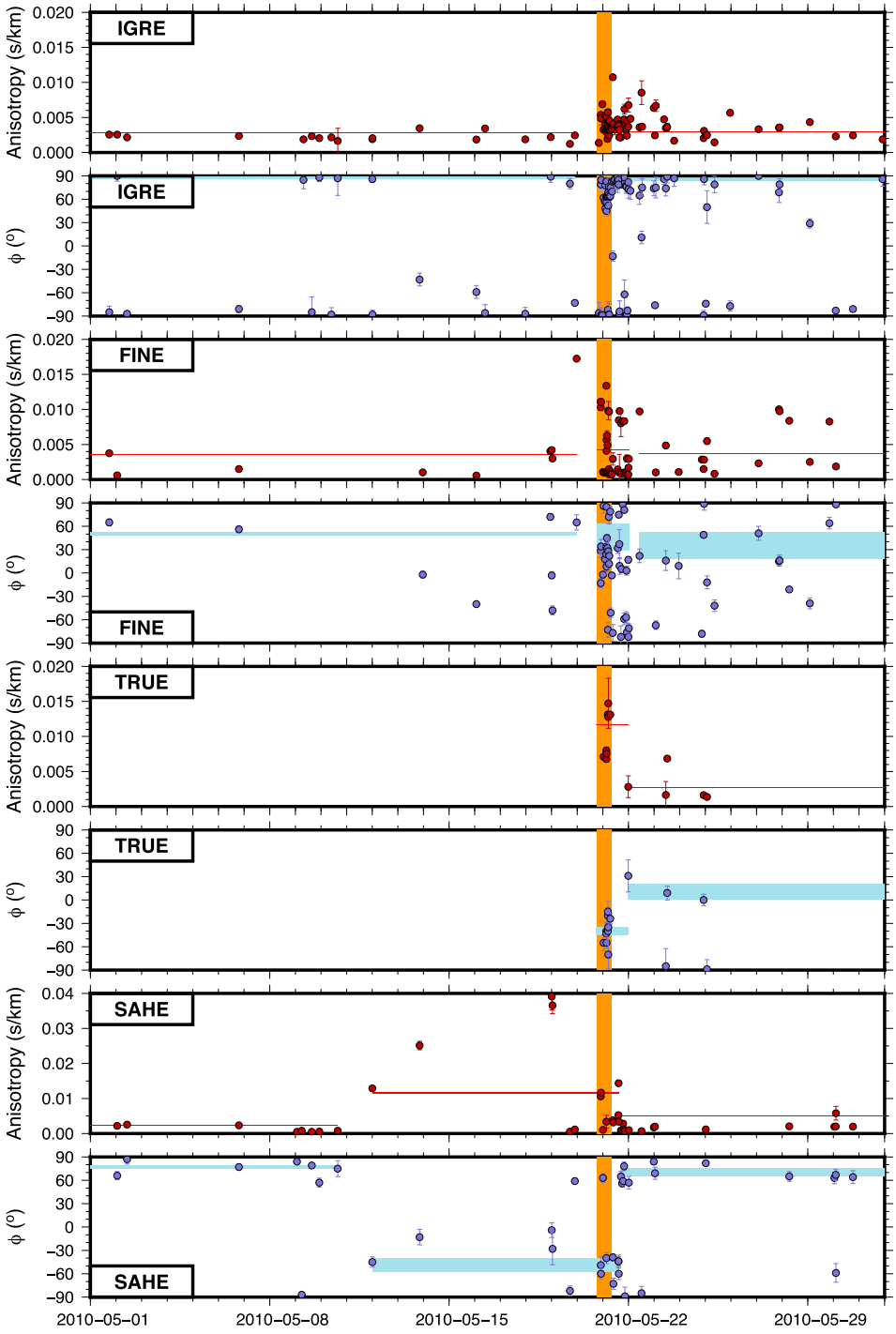

Figure 6. Seismic anisotropy through time at IGRE, FINE, TRUE and SAHE for may 2010. Colored background boxes indicate the mean value ± error, before, during and after the dyke intrusion. Orange box indicates time at which the dyke was intruding. Note the different Y axis for anisotropy (s/km) at SAHE.

distances (Figure 7); thus, individual raypaths will traverse mediums with different anisotropic properties. Studies of shear-wave splitting in vertically heterogenous anisotropic medium show that the observed anisotropy orientation is weighted toward the anisotropy in the upper layer (Rümpker & Silver, 1998; Saltzer et al. (2000)). In our study, the upper layer corresponds to the anisotropy near the station; thus, we compare observed seismic anisotropy to the modeled SH_{max} orientation near the station. This

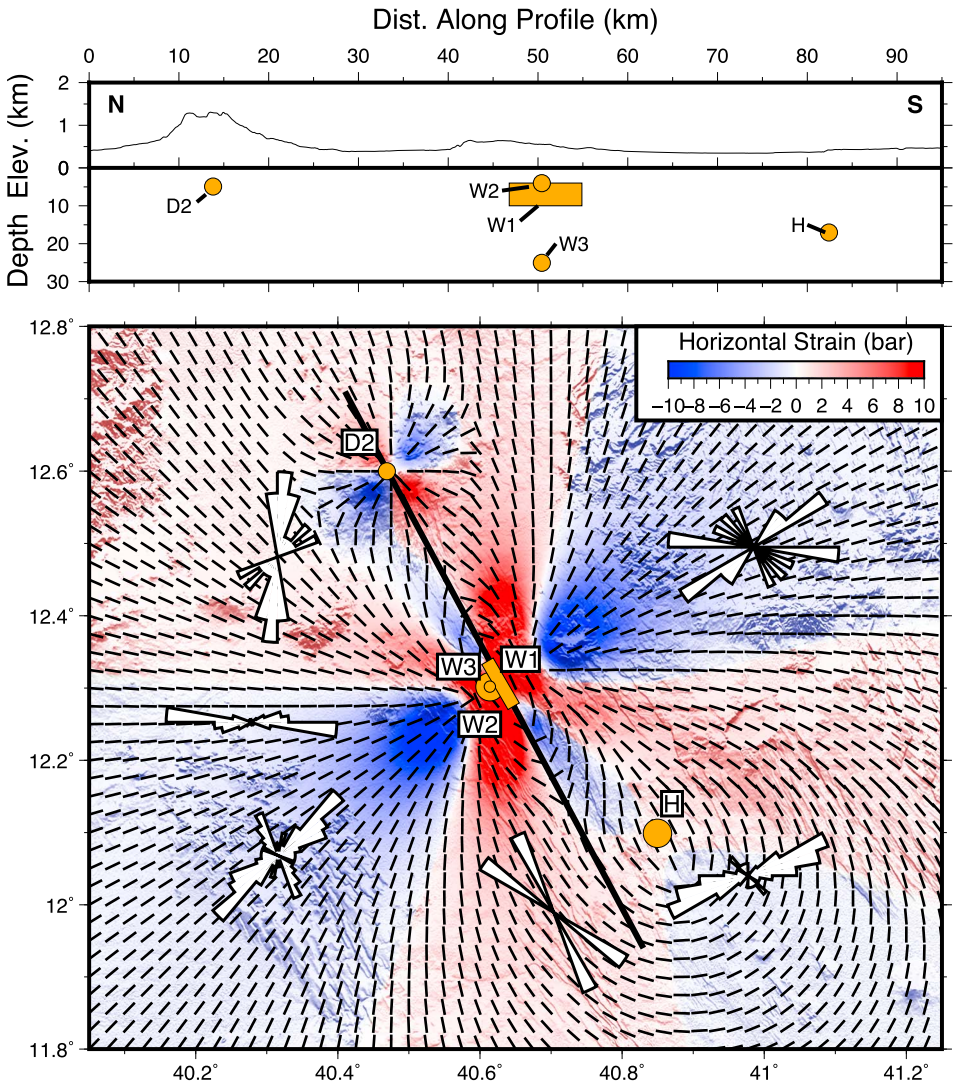

Figure 7. Stress modeling of the deforming magmatic bodies identified by Grandin, Socquet, Doin, et al. (2010). The small black bars show the modeled orientation of the maximum horizontal stress. The rose plots show the predyke anisotropy orientations (Figure 4a). The black line denotes the profile for the cross section.

comparison shows that the predyke anisotropy orientations can be well explained by the stresses that are induced by the deforming magma bodies. The magmatic feature, which is found to have the greatest impact on the stress field, is the inflating, dyke-like body (W1), which forms part of the AVC magmatic segment. This induces an anisotropy pattern that is roughly radial to the rift center (Figure 7). Stations SAHE and TRUE appear to be affected by magma bodies H and D2, respectively. Body H is a deep, deflating magma chamber, which induces a circular anisotropy in the surrounding region. This best explains the ENE-WSW anisotropy at SAHE (Figure 7). Body D2 is an inflating magma chamber beneath Dabbahu volcano and induces radial anisotropy in the surrounding region. All the earthquakes, which yield anisotropy measurements at TRUE, originate in the north of the rift segment, to the east of TRUE (Figure 4a). Consequently, this means that the associated raypaths will travel through the region (~12.5, 40.5) characterized by ~N-S anisotropy, and high strain, induced by D2 (Figure 7). This region of N-S oriented anisotropy will dominate (Figure S3), thus causing the anisotropy orientation at TRUE to be ~N-S.

4.2. Precursory Changes

Previous studies of seismic anisotropy have suggested that it can be used as a precursor to forecast future eruptions (e.g., Bianco et al., 2006; Gerst & Savage, 2004; Volti & Crampin, 2003). The data from the

Dabbahu segment do not conclusively display a precursory change in seismic anisotropy before the May 2010 dyke intrusion and associated fissure eruption (Figures 5 and 6). Stations TRUE and IGRE show no obvious change in either delay time or anisotropy orientation until the initiation of the dyke intrusion. At TRUE this may be due to a lack of data points between 23:25:16, 13 May 2010 and the start of dyke intrusion (18:09:00, 20 May 2010); however, at IGRE there is frequent data in the days preceding the dyke intrusion (Figure 6). FINE does not show an obvious precursory change in anisotropy, with the exception of a measurement at 23:31:44, 19 May 2010, approximately 18 hr before the start of the dyke intrusion. This measurement records a delay time of 0.017 s/km, which is the highest recorded during the entire recording period at FINE.

In contrast, SAHE shows a clear precursory change in seismic anisotropy leading up to the dyke intrusion. At 00:12:55, 12 May 2010 seismic anisotropy changes from an average orientation of ~79° and average delay time of 0.0056 s/km, to record a measurement of −45° and 0.013 s/km (Figure 6). The delay time continues to increase, and the anisotropy orientation remains ~ −45° until 17:15:56, 19 May 2010, approximately 23 hr before the dyke intrusion, when the delay time drops dramatically (Figure 6). There are relatively few measurements prior to the dyke intrusion; thus, we must make interpretations with care. If we consider the precursory measurements as a whole, allowing for scatter of individual measurements, then the change in anisotropy orientation to −45° ± 9° is significant. It is interesting to note that this precursory change in seismic anisotropy is only clearly observed at SAHE. If the change in anisotropy was induced by deformation at the center of the Dabbahu segment, one would expect this to occur at all of the proximal stations, as all are a similar distance from the Dabbahu segment center (Figure 2). As the precursory change is only observed at SAHE, we suggest that the cause is more local to this station. The orientation of anisotropy at SAHE prior to the dyke intrusion is controlled by the deflating source at Hararo (H; Figure 7). This deflation induces a circular horizontal stress pattern, causing the NE-SW oriented anisotropy at SAHE. If the Hararo magma chamber were to begin inflating, it would induce a radial stress pattern, which would manifest as NW-SE oriented anisotropy at SAHE.

In addition to the change in anisotropy at SAHE, we note that there is an increased level of seismicity in the Hararo region (Figure 2). We manually refine the arrival time picks and relocate seismicity located close to the Hararo deformation source using NonLinLoc (Lomax et al., 2000) and a 1-D velocity model for the Dabbahu region (Belachew et al., 2011). This reveals that seismicity near the Hararo magma chamber is anomalously deep (>15 km) with an average error in depth of ±3.8 km. These earthquakes occur significantly deeper than the proposed brittle-ductile transition at 8 to 10 km depth (Ebinger et al., 2008; Figure 8). The deep seismicity occurs in a swarm like pattern (Figure 8), with the first swarm initiating on 13 May 2010, the day after seismic anisotropy measurements at SAHE are observed to change dramatically. These combined observations provide good evidence that the Hararo deformation source begins to deform and inflate on 12 May 2010.

The change in deformation style at Hararo may be a precursor to the dyke intrusion and fissure eruption in the Dabbahu segment. Grandin, Socquet, Doin, et al. (2010) observed that there is a volume balance between the long-term deflation signal at the lower crustal Hararo magma chamber (*H*) and the lower crustal Wal'lis magma chamber (W3). They used this to suggest that the two magma reservoirs may be hydraulically connected. Grandin, Socquet, Doin, et al. (2010) suggest that the dyke intrusions in the Dabbahu segment between 2005 and 2010 sourced magma from the deep Wal'lis magma reservoir, causing a decrease in pressure and an inflow of magma. This inflow of magma may be sourced from the deflating Hararo magma reservoir in the neighboring magmatic segment. In this sense, the deflation at Hararo is driven by low pressure in the Wal'lis magma reservoir. Therefore, if the Wal'lis magma chamber were to become overpressured, one would expect the Hararo magma reservoir to cease deflating and begin inflating. Therefore, the inflation of the Hararo magma chamber, beginning 12 May 2010, indicates that the Wal'lis magma chamber had become overpressured. This overpressure was then released with the migration of magma from the Wal'lis reservoir to the shallow plumbing system beneath the Dabbahu segment and the subsequent dyke intrusion and fissure eruption. In this sense, the dramatic change in anisotropy magnitude and orientation observed at SAHE records a precursory signal that the Wal'lis magma reservoir is overpressured and that an eruption/dyke intrusion may be imminent.

Our results build on a growing body of evidence, which suggests that the magmatic system beneath the Dabbahu segment is fed by significant lateral flow of magma in the lower crust from the Manda Hararo segment. This occurs over distances of approximately 35 km and appears to dynamically respond to pressure

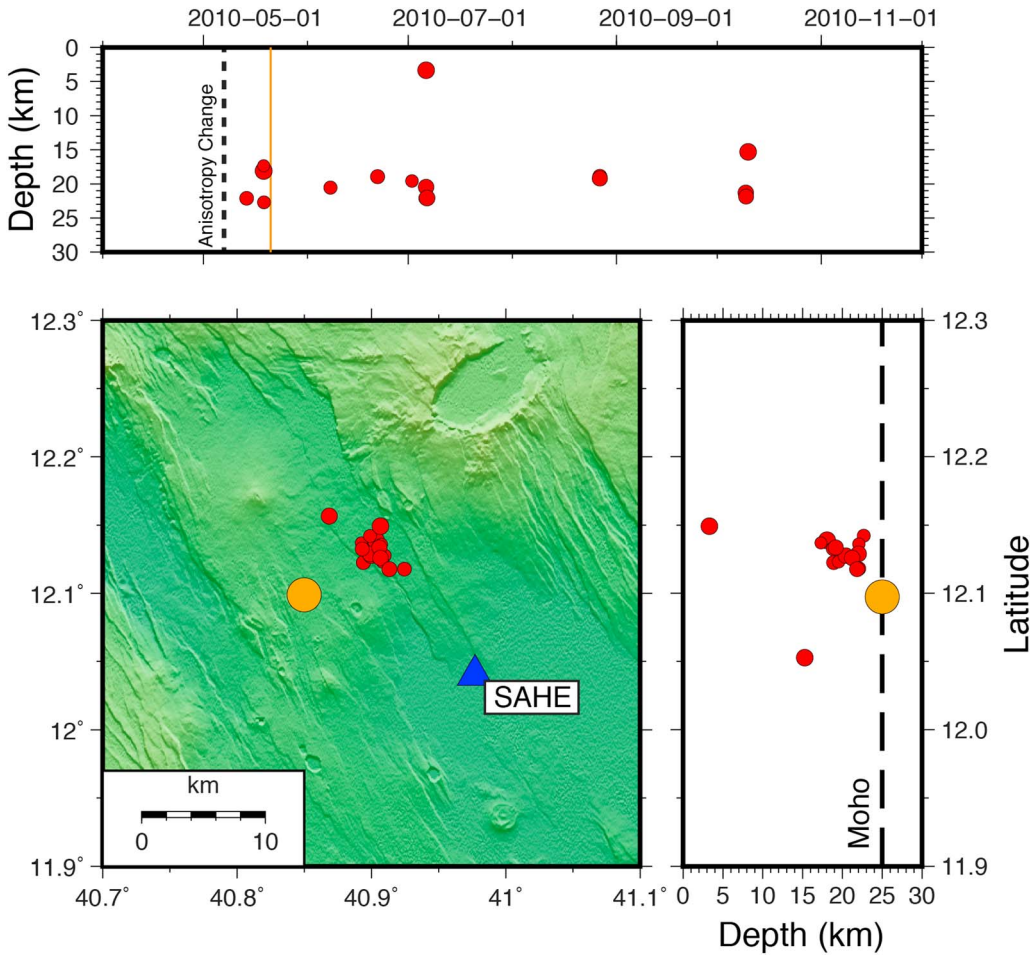

Figure 8. Relocated seismicity in the vicinity of the lower crustal Hararo deformation source. Deep seismicity begins on 13 May 2010, shortly after the orientation and magnitude of anisotropy is observed to change at SAHE. Average errors in depth are ±3.8 km.

changes in the magma plumbing system. These findings suggest that magmatic segments in continental rifts are not necessarily isolated systems and that rift segments can interact through the direct transfer of magmatic material.

4.3. Codyke Anisotropy

We can further model the horizontal stress that is induced by the intrusion of the May 2010 dyke. We use dyke parameters obtained from deformation modeling by Barnie et al. (2015) and compare the model results to observations of seismic anisotropy during the dyke intrusion. We find that there is excellent agreement between the modeled orientation of maximum horizontal stress and the observed orientation of seismic anisotropy (Figure 9). The modeled, dyke-induced stress field is similar to that modeled for the interdyke stress (Figure 7); this is largely due to the elongate, inflating magma source W1 beneath the AVC. It is not known whether the magma bodies identified by Grandin, Socquet, Doin, et al. (2010) and modeled in Figure 7, continue to deform during the dyke intrusion. However, the excellent agreement between the modeled, dyke-induced stress and the codyke anisotropy suggests that the dyke dominates the stress field while it is intruding. In addition, we observe that during the dyke intrusion, the magnitude of anisotropy increases by an average ratio of 2.03 (Table 1), indicating that the intrusion affects the seismic anisotropy. As seismic anisotropy is accrued along the entire earthquake raypath, it is difficult to distinguish whether the increase in anisotropy occurs close to the intrusion or in the surrounding region. Two possible models could explain the codyke anisotropy observations. In the first model, the intrusion of new magmatic material would

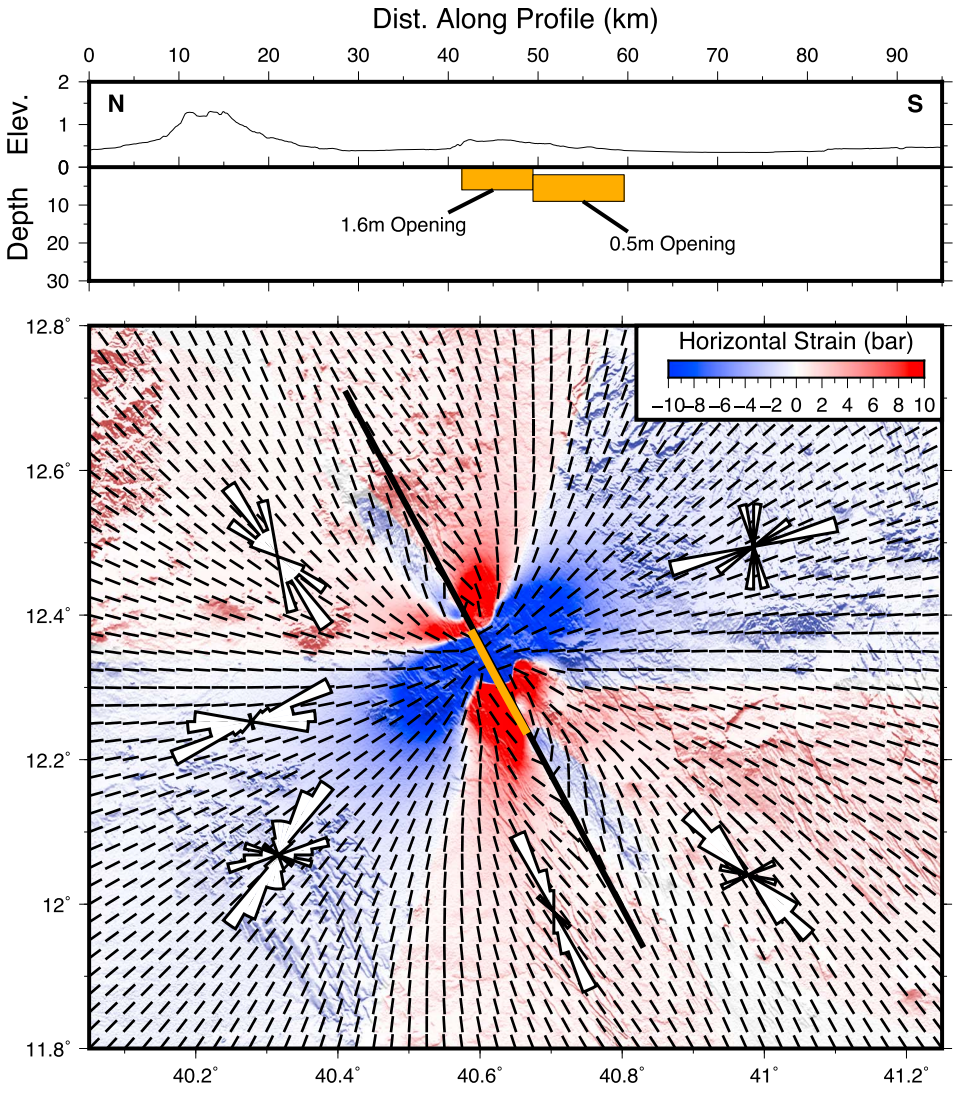

Figure 9. Stress modeling of the May 2010 dyke intrusion with parameters taken from Barnie et al. (2015). The small black bars show the modeled orientation of the maximum horizontal stress. The rose plots show the codyke anisotropy orientations (Figure 4b). The black line denotes the profile for the cross section.

increase the horizontal stress in the surrounding region, increasing the aspect ratio of microcracks and causing an increase in shear-wave delay times (Crampin, 1994). Alternatively, the dyke intrusion will cause an increase in temperature in the highly active hydrothermal system of the Dabbahu segment (Figures 1 and 2; Keir et al., 2009). This will increase the fluid pressure on a local scale and cause an increase in the magnitude of seismic anisotropy within the Dabbahu segment (Elkibbi et al., 2005; Johnson & Savage, 2012). Both mechanisms of increasing the magnitude of seismic anisotropy could be acting simultaneously, and it is difficult to distinguish between them by considering the codyke anisotropy. However, insight may be gained through studying how the seismic anisotropy evolves once the dyke has ceased propagating.

4.4. Reversal of Anisotropy

We observe that the anisotropy orientation and delay time revert back to predyke values after the dyke has ceased propagating (Figure 5). At FINE there is a delay of ~8 hr between the end of dyke propagation and the reversal of anisotropy values (Figure 6). Where anisotropy has been observed to change in response to magmatic activity in other regions (e.g., Gerst & Savage, 2004; Volti & Crampin, 2003), the anisotropy takes significantly longer to return to previous values (months to years). Volti and Crampin (2003) suggest that

this time delay is due to the time it takes for the surrounding rock mass to accommodate the strain induced by the emplacement of magmatic material. The May 2010 dyke intrusion induced opening of 1–1.6 m (Barnie et al., 2015). Pagli et al. (2014) have found that opening rates in the Dabbahu region are up to 110 mm/year; in response to the rifting episode, it is therefore unlikely that the stress induced by the May 2010 dyke could be accommodated by plate spreading in such a short amount of time.

Studies of anisotropy that varies with large earthquakes have observed that the anisotropy returns to background values immediately after the earthquake, interpreted as indicating a release of stress in the earthquake rupture (Peacock et al., 1988; Volti & Crampin, 2003). The May 2010 eruption induced many earthquakes, which resulted in a cumulative seismic moment release of 1.208×10^{16} Nm (Figure 3). This induced seismicity will have released a proportion of the stress induced by the dyke intrusion, potentially explaining the quick reversal of seismic anisotropy. However, Barnie et al. (2015) calculate the total geodetic moment of the dyke intrusion to be 3.216×10^{18} Nm, two orders of magnitude greater than the seismic moment release. It therefore appears unlikely that the induced seismicity can release the dyke-induced stress and explain the quick anisotropy reversal.

As discussed previously, the increase in seismic anisotropy magnitude observed during the dyke intrusion could be caused by either the intrusion of magmatic material increasing the regional horizontal stress or an increase in temperature and pressure in the hydrothermal system of the Dabbahu segment. For the reasons discussed above, it seems unlikely that an increase in regional horizontal stress could be dissipated on the time-scales which we observe the seismic anisotropy to return to predyke values. We therefore suggest that the increase in magnitude of seismic anisotropy that we observe during the dyke intrusion is caused by the heating and pressurization of the Dabbahu hydrothermal system, while the orientation of these fluid-filled cracks is controlled by the codyke stress field (Figure 9). Finally, we observe that the anisotropy orientation at SAHE returns to a NE-SW orientation after the dyke intrusion (Figures 4 and 5). Building on our previous discussions, this suggests that the Hararo magma reservoir resumed deflation after the dyke intrusion. We can infer that this is in response to the withdrawal of magma beneath the Dabbahu segment causing a decrease in pressure at the Wal'lis magma reservoir.

5. Conclusion

We present a detailed study of the crustal seismic anisotropy of the Dabbahu magmatic rift segment between October 2009 and October 2010. Our data have a high temporal resolution and allow us to document how seismic anisotropy varies through time in response a dyke intrusion in May 2010. Our key findings are as follows:

1. Seismic anisotropy prior to the May 2010 dyke intrusion is controlled by the deforming magma plumbing system of the Dabbahu rift segment and not by far field tectonic stresses.
2. Through modeling of magmatically induced stress we show that our seismic anisotropy results are in broad agreement with previous models of the magma plumbing system.
3. Seismic anisotropy shows that a deep magma reservoir in the adjacent Manda-Hararo segment began to inflate approximately eight days prior to the dyke intrusion in the Dabbahu segment.
4. During the dyke intrusion the magnitude of seismic anisotropy increases, suggesting a pressurization of the hydrothermal system within the Dabbahu segment.

Our results provide strong evidence that the Dabbahu and Manda-Hararo magmatic segments are hydraulically connected. The seismic anisotropy results presented here were able to detect a change in deformation in a deep magma reservoir in the Manda-Hararo segment. This observation can be used to infer an overpressure within the Wal'lis magma reservoir, in the Dabbahu segment, and potentially to forecast impending magmatic activity.

Acknowledgments
We thank SEIS-UK for use of the instruments and their computing facilities. The facilities of SEIS-UK are supported by the Natural Environment Research Council (NERC) under agreement R8/H10/64. F. I. K. is funded through NERC studentship NE/L002531/1, a grant to GSNOCS from Roy Franklin O.B.E. and the ECLIPSE program funded by the New Zealand Ministry of Business Innovation and Employment. D. K. and T. G. are supported by NERC grant NE/L013932. Funding for fieldwork is from BHP Billiton. We also acknowledge assistance from Addis Ababa University and the Afar National Regional State Government. The MFAST package is available for download at http://mfast-package.geo.vuw.ac.nz. We thank Talfan Barnie for providing the effusion rate data and Jessica Johnson for useful discussions. We would like to thank Zefeng Li and an anonymous reviewer for providing constructive reviews which helped to improve the manuscript. The earthquake location and seismic anisotropy data is provided in the supporting information.

References

Ahmed, A., Doubre, C., Leroy, S., Kassim, M., Keir, D., Abayazid, A., Julie, P., et al. (2016). Seafloor spreading event in western Gulf of Aden during the November 2010–March 2011 period captured by regional seismic networks: Evidence for diking events and interactions with a nascent transform zone. *Geophysical Journal International*, *205*(2), 1244–1266. https://doi.org/10.1093/gji/ggw068

Aster, R. C., Shearer, P. M., & Berger, J. (1990). Quantitative measurements of shear wave polarizations at the Anza seismic network, southern California: Implications for shear wave splitting and earthquake prediction. *Journal of Geophysical Research*, *95*(B8), 12,449–12,473. https://doi.org/10.1029/JB095iB08p12449

Ayalew, D., Ebinger, C., Bourdon, E., Wolfenden, E., Yirgu, G., & Grassineau, N. (2006). Temporal compositional variation of syn-rift rhyolites along the western margin of the southern Red Sea and northern Main Ethiopian Rift. *Geological Society of London, Special Publication*, *259*(1), 121–130. https://doi.org/10.1144/GSL.SP.2006.259.01.10

Ayele, A., Stuart, G., Bastow, I., & Keir, D. (2007). The August 2002 earthquake sequence in north Afar: Insights into the neotectonics of the Danakil microplate. *Journal of African Earth Sciences*, *40*, 70–79.

Barnie, T. D., Keir, D., Hamling, I., Hofmann, B., Belachew, M., Carn, S., Eastwell, D., et al. (2015). A multidisciplinary study of the final episode of the Manda Hararo dyke sequence, Ethiopia, and implications for trends in volcanism during the rifting cycle. *Geological Society of London, Special Publication*, *420*, SP420–SP426.

Bastow, I., Pilidou, S., Kendall, J.-M., & Stuart, G. (2010). Melt-induced seismic anisotropy and magma assisted rifting in Ethiopia: Evidence from surface waves. *Geochemistry, Geophysics, Geosystems*, *11*, Q0AB05. https://doi.org/10.1029/2010GC003036

Belachew, M., Ebinger, C., Coté, D., Keir, D., Rowland, J., Hammond, J., & Ayele, A. (2011). Comparison of dike intrusions in an incipient seafloor-spreading segment in Afar, Ethiopia: Seismicity perspectives. *Journal of Geophysical Research*, *116*, B06405. https://doi.org/10.1029/2010JB007908

Bianco, F., Scarfì, L., Del Pezzo, E., & Patanè, D. (2006). Shear wave splitting time variation by stress-induced magma uprising at Mount Etna volcano. *Geophysical Journal International*, *67*, 59–967.

Boness, N. L., & Zoback, M. D. (2006). Mapping stress and structurally controlled crustal shear velocity anisotropy in California. *Geology*, *34*(10), 825–828. https://doi.org/10.1130/G22309.1

Booth, D., & Crampin, S. (1985). Shear-wave polarizations on a curved wavefront at an isotropic free surface. *Geophysical Journal of the Royal Astronomical Society*, *83*(1), 31–45. https://doi.org/10.1111/j.1365-246X.1985.tb05154.x

Crampin, S. (1984). An introduction to wave propagation in anisotropic media. *Geophysical Journal International*, *76*(1), 17–28. https://doi.org/10.1111/j.1365-246X.1984.tb05018.x

Crampin, S. (1987). Geological and industrial implications of extensive-dilatancy anisotropy. *Nature*, *328*(6130), 491–496. https://doi.org/10.1038/328491a0

Crampin, S. (1994). The fracture criticality of crustal rocks. *Geophysical Journal International*, *118*(2), 428–438. https://doi.org/10.1111/j.1365-246X.1994.tb03974.x

Crampin, S. (1999). Calculable fluid–rock interactions. *Journal of the Geological Society*, *156*(3), 501–514. https://doi.org/10.1144/gsjgs.156.3.0501

Crampin, S., Booth, D. C., Evans, R., Peacock, S., & Fletcher, J. B. (1991). Comment on "Quantitative measurements of shear wave polarizations at the Anza seismic network, southern California: Implications for shear wave splitting and earthquake prediction" by Richard C. Aster, Peter M. Shearer, and Jon Berger. *Journal of Geophysical Research*, *96*(B4), 6403–6414. https://doi.org/10.1029/90JB02453

Crampin, S., & Peacock, S. (2008). A review of the current understanding of seismic shear-wave splitting in the Earth's crust and common fallacies in interpretation. *Wave Motion*, *45*(6), 675–722. https://doi.org/10.1016/j.wavemoti.2008.01.003

Crampin, S., & Zatsepin, S. V. (1997). Modelling the compliance of crustal rock. Response to temporal changes before earthquakes. *Geophysical Journal International*, *129*(3), 495–506. https://doi.org/10.1111/j.1365-246X.1997.tb04489.x

Crotwell, H. P., Owens, T., & Ritsema, J. (1999). The TauP Toolkit: Flexible seismic travel-time and ray-path utilities. *Seismological Research Letters*, *70*(2), 154–160. https://doi.org/10.1785/gssrl.70.2.154

Drew, J., White, R. S., Tilmann, F., & Tarasewicz, J. (2013). Coalescence microseismic mapping. *Geophysical Journal International*, *195*(3), 1773–1785. https://doi.org/10.1093/gji/ggt331

Dunn, R. A., Lekic, V., Detrick, R. S., & Toomey, D. R. (2005). Three-dimensional seismic structure of the Mid-Atlantic Ridge (35°N): Evidence for focused melt supply and lower crustal dike injection. *Journal of Geophysical Research*, *110*, B09101. https://doi.org/10.1029/2004JB003473

Ebinger, C. J., Keir, D., Ayele, A., Calais, E., Wright, T. J., Belachew, M., Hammond, J. O., et al. (2008). Capturing magma intrusion and faulting processes during continental rupture: Seismicity of the Dabbahu (Afar) rift. *Geophysical Journal International*, *174*(3), 1138–1152. https://doi.org/10.1111/j.1365-246X.2008.03877.x

Elkibbi, M., Yang, M., & Rial, J. (2005). Crack-induced anisotropy models in The Geysers geothermal field. *Geophysical Journal International*, *162*(3), 1036–1048. https://doi.org/10.1111/j.1365-246X.2005.02697.x

Field, L., Barnie, T., Blundy, J., Brooker, R. A., Keir, D., Lewi, E., & Saunders, K. (2012). Integrated field, satellite and petrological observations of the November 2010 eruption of Erta Ale. *Bulletin of Volcanology*, *74*(10), 2251–2271. https://doi.org/10.1007/s00445-012-0660-7

Gerst, A., & Savage, M. K. (2004). Seismic anisotropy beneath Ruapehu volcano: A possible eruption forecasting tool. *Science*, *306*(5701), 1543–1547. https://doi.org/10.1126/science.1103445

Grandin, R., Socquet, A., Doin, M.-P., Jacques, E., de Chabalier, J.-B., & King, G. (2010). Transient rift opening in response to multiple dike injections in the Manda Hararo rift (Afar, Ethiopia) imaged by time-dependent elastic inversion of interferometric synthetic aperture radar data. *Journal of Geophysical Research*, *115*, B09403. https://doi.org/10.1029/2009JB006883

Grandin, R., Socquet, A., Jacques, E., Mazzoni, N., de Chabalier, J.-B., & King, G. (2010). Sequence of rifting in Afar, Manda-Hararo rift, Ethiopia, 2005–2009: Time-space evolution and interactions between dikes from interferometric synthetic aperture radar and static stress change modeling. *Journal of Geophysical Research*, *115*, B10413. https://doi.org/10.1029/2009JB000815

Greenfield, T., White, R. S., & Roecker, S. (2016). The magmatic plumbing system of the Askja central volcano, Iceland, as imaged by seismic tomography. *Journal of Geophysical Research: Solid Earth*, *121*, 7211–7229. https://doi.org/10.1002/2016JB013163

Hamling, I., Ayele, A., Bennati, L., Calais, E., Ebinger, C., Keir, D., Lewi, E., et al. (2009). Geodetic observations of the ongoing Dabbahu rifting episode: New dyke intrusions in 2006 and 2007. *Geophysical Journal International*, *178*(2), 989–1003. https://doi.org/10.1111/j.1365-246X.2009.04163.x

Hamling, I. J., Wright, T. J., Calais, E., Bennati, L., & Lewi, E. (2010). Stress transfer between thirteen successive dyke intrusions in Ethiopia. *Nature Geoscience*, *3*(10), 713–717. https://doi.org/10.1038/ngeo967

Hayward, N., & Ebinger, C. (1996). Variations in the along–axis segmentation of the Afar rift system. *Tectonics*, *15*(2), 244–257. https://doi.org/10.1029/95TC02292

Illsley-Kemp, F., Keir, D., Bull, J. M., Ayele, A., Hammond, J. O., Kendall, J.-M., Gallacher, R. J., et al. (2017). Local earthquake magnitude scale and b-value for the Danakil region of northern Afar. *Bulletin of the Seismological Society of America*, *107*(2), 521–531. https://doi.org/10.1785/0120150253

Illsley-Kemp, F., Keir, D., Bull, J. M., Gernon, T. M., Ebinger, C., Ayele, A., Hammond, J. O., et al. (2018). Seismicity during continental breakup in the Red Sea rift of northern Afar. *Journal of Geophysical Research: Solid Earth*, *123*, 2345–2362. https://doi.org/10.1002/2017JB014902

Illsley-Kemp, F., Savage, M. K., Keir, D., Hirschberg, H. P., Bull, J. M., Gernon, T. M., Hammond, J. O., et al. (2017). Extension and stress during continental breakup: Seismic anisotropy of the crust in northern Afar. *Earth and Planetary Science Letters*, *477*, 41–51. https://doi.org/10.1016/j.epsl.2017.08.014

Johnson, J. H., & Savage, M. K. (2012). Tracking volcanic and geothermal activity in the Tongariro volcanic Centre, New Zealand, with shear wave splitting tomography. *Journal of Volcanology and Geothermal Research*, *223*, 1–10.

Johnson, J. H., Savage, M. K., & Townend, J. (2011). Distinguishing between stress-induced and structural anisotropy at Mount Ruapehu Volcano, New Zealand. *Journal of Geophysical Research*, *116*, B12303. https://doi.org/10.1029/2011JB008308

Keir, D., Bastow, I. D., Whaler, K. A., Daly, E., Cornwell, D. G., & Hautot, S. (2009). Lower crustal earthquakes near the Ethiopian rift induced by magmatic processes. *Geochemistry, Geophysics, Geosystems*, *10*, Q0AB02. https://doi.org/10.1029/2009GC002382

Keir, D., Belachew, M., Ebinger, C., Kendall, J.-M., Hammond, J. O. S., Stuart, G. W., Ayele, A., et al. (2011). Mapping the evolving strain field during continental breakup from crustal anisotropy in the Afar depression. *Nature Communications*, *2*(1), 285. https://doi.org/10.1038/ncomms1287

Keir, D., Kendall, J.-M., Ebinger, C., & Stuart, G. (2005). Variations in late syn-rift melt alignment inferred from shear-wave splitting in crustal earthquakes beneath the Ethiopian rift. *Geophysical Research Letters*, *32*, L23308. https://doi.org/10.1029/2005GL024150

Li, Z., & Peng, Z. (2017). Stress-and structure-induced anisotropy in Southern California from two decades of shear wave splitting measurements. *Geophysical Research Letters*, *44*, 9607–9614. https://doi.org/10.1002/2017GL075163

Li, Z., Zhang, H., & Peng, Z. (2014). Structure-controlled seismic anisotropy along the Karadere–Düzce branch of the North Anatolian Fault revealed by shear-wave splitting tomography. *Earth and Planetary Science Letters*, *391*, 319–326. https://doi.org/10.1016/j.epsl.2014.01.046

Lin, J., & Stein, R. S. (2004). Stress triggering in thrust and subduction earthquakes and stress interaction between the southern San Andreas and nearby thrust and strike-slip faults. *Journal of Geophysical Research*, *109*, B02303. https://doi.org/10.1029/2003JB002607

Lomax, A., Virieux, J., Volant, P., & Berge-Thierry, C. (2000). Probabilistic earthquake location in 3D and layered models. In *Advances in Seismic Event Location* (pp. 101–134). Dordrecht, Netherlands: Springer.

Manighetti, I., Tapponnier, P., Courtillot, V., Gallet, Y., Jacques, E., & Gillot, P.-Y. (2001). Strain transfer between disconnected, propagating rifts in Afar. *Journal of Geophysical Research*, *106*(B7), 13,613–13,665. https://doi.org/10.1029/2000JB900454

Mardia, K. V., & Jupp, P. E. (2000). *Directional Statistics*. Chichester, UK: John Wiley.

McKenzie, D., & Davies, D. (1970). Plate tectonics of the Red Sea and east Africa. *Nature*, *226*(5242), 243–248. https://doi.org/10.1038/226243a0

Medynski, S., Pik, R., Burnard, P., Dumont, S., Grandin, R., Williams, A., Blard, P.-H., et al. (2016). Magmatic cycles pace tectonic and morphological expression of rifting (Afar depression, Ethiopia). *Earth and Planetary Science Letters*, *446*, 77–88. https://doi.org/10.1016/j.epsl.2016.04.014

Medynski, S., Pik, R., Burnard, P., Williams, A., Vye-Brown, C., Ferguson, D., Blard, P.-H., et al. (2013). Controls on magmatic cycles and development of rift topography of the Manda Hararo segment (Afar, Ethiopia): Insights from cosmogenic 3He investigation of landscape evolution. *Earth and Planetary Science Letters*, *367*, 133–145. https://doi.org/10.1016/j.epsl.2013.02.006

Menke, W., Brandsdottir, B., Jakobsdottir, S., & Stefansson, R. (1994). Seismic anisotropy in the crust at the mid-Atlantic plate boundary in South-West Iceland. *Geophysical Journal International*, *119*(3), 783–790. https://doi.org/10.1111/j.1365-246X.1994.tb04017.x

Miller, V., & Savage, M. (2001). Changes in seismic anisotropy after volcanic eruptions: Evidence from Mount Ruapehu. *Science*, *293*(5538), 2231–2233. https://doi.org/10.1126/science.1063463

Pagli, C., Wang, H., Wright, T. J., Calais, E., & Lewi, E. (2014). Current plate boundary deformation of the Afar rift from a 3-D velocity field inversion of InSAR and GPS. *Journal of Geophysical Research: Solid Earth*, *119*, 8562–8575. https://doi.org/10.1002/2014JB011391

Peacock, S., Crampin, S., Booth, D. C., & Fletcher, J. B. (1988). Shear wave splitting in the Anza seismic gap, southern California: Temporal variations as possible precursors. *Journal of Geophysical Research*, *93*(B4), 3339–3356. https://doi.org/10.1029/JB093iB04p03339

Roman, D. C., Savage, M. K., Arnold, R., Latchman, J. L., & De Angelis, S. (2011). Analysis and forward modeling of seismic anisotropy during the ongoing eruption of the Soufrière Hills Volcano, Montserrat, 1996–2007. *Journal of Geophysical Research*, *116*, B03201. https://doi.org/10.1029/2010JB007667

Rümpker, G., & Silver, P. G. (1998). Apparent shear-wave splitting parameters in the presence of vertically varying anisotropy. *Geophysical Journal International*, *135*(3), 790–800. https://doi.org/10.1046/j.1365-246X.1998.00660.x

Saltzer, R. L., Gaherty, J. B., & Jordan, T. H. (2000). How are vertical shear wave splitting measurements affected by variations in the orientation of azimuthal anisotropy with depth? *Geophysical Journal International*, *141*(2), 374–390. https://doi.org/10.1046/j.1365-246x.2000.00088.x

Savage, M., Ferrazzini, V., Peltier, A., Rivemale, E., Mayor, J., Schmid, A., Brenguier, F., et al. (2015). Seismic anisotropy and its precursory change before eruptions at Piton de la Fournaise volcano, La Réunion. *Journal of Geophysical Research: Solid Earth*, *120*, 3430–3458. https://doi.org/10.1002/2014JB011665

Savage, M., Wessel, A., Teanby, N., & Hurst, A. (2010). Automatic measurement of shear wave splitting and applications to time varying anisotropy at Mount Ruapehu volcano, New Zealand. *Journal of Geophysical Research*, *115*, B12321. https://doi.org/10.1029/2010JB007722

Silver, P., & Chan, G. (1991). Shear wave splitting and subcontinental mantle deformation. *Journal of Geophysical Research*, *96*(B10), 16,429–16,454. https://doi.org/10.1029/91JB00899

Tan, Y. J., Tolstoy, M., Waldhauser, F., & Wilcock, W. S. (2016). Dynamics of a seafloor-spreading episode at the East Pacific Rise. *Nature*, *540*(7632), 261–265. https://doi.org/10.1038/nature20116

Tang, C., Rial, J. A., & Lees, J. M. (2005). Shear-wave splitting: A diagnostic tool to monitor fluid pressure in geothermal fields. *Geophysical Research Letters*, *32*, L21317. https://doi.org/10.1029/2005GL023551

Teanby, N., Kendall, J.-M., & van der Baan, M. (2004). Automation of shear-wave splitting measurements using cluster analysis. *Bulletin of the Seismological Society of America*, *94*(2), 453–463. https://doi.org/10.1785/0120030123

Temtime, T., Biggs, J., Lewi, E., Hamling, I., Wright, T., & Ayele, A. (2018). Spatial and temporal patterns of deformation at the Tendaho geothermal prospect, Ethiopia. *Journal of Volcanology and Geothermal Research*, *357*, 56–67. https://doi.org/10.1016/j.jvolgeores.2018.04.004

Toda, S., Stein, R. S., Richards-Dinger, K., & Bozkurt, S. B. (2005). Forecasting the evolution of seismicity in southern California: Animations built on earthquake stress transfer. *Journal of Geophysical Research*, *110*, B05S16. https://doi.org/10.1029/2004JB003415

Volti, T., & Crampin, S. (2003). A four-year study of shear-wave splitting in Iceland: 2. Temporal changes before earthquakes and volcanic eruptions. *Geological Society of London, Special Publication*, *212*(1), 135–149. https://doi.org/10.1144/GSL.SP.2003.212.01.09

Woessner, J., & Wiemer, S. (2005). Assessing the quality of earthquake catalogues: Estimating the magnitude of completeness and its uncertainty. *Bulletin of the Seismological Society of America*, *95*(2), 684–698. https://doi.org/10.1785/0120040007

Wolfenden, E., Ebinger, C., Yirgu, G., Renne, P., & Kelley, S. (2005). Evolution of a volcanic rifted margin: Southern Red Sea, Ethiopia. *Bulletin Geological Society of America*, *117*(7), 846–864. https://doi.org/10.1130/B25516.1

Wright, T., Ebinger, C., Biggs, J., Ayele, A., Yirgu, G., Keir, D., & Stork, A. (2006). Magma-maintained rift segmentation at continental rupture in the 2005 Afar dyking episode. *Nature*, *442*(7100), 291–294. https://doi.org/10.1038/nature04978

Wright, T. J., Sigmundsson, F., Pagli, C., Belachew, M., Hamling, I. J., Brandsdóttir, B., Keir, D., et al. (2012). Geophysical constraints on the dynamics of spreading centres from rifting episodes on land. *Nature Geoscience*, *5*(4), 242–250. https://doi.org/10.1038/ngeo1428

Zinke, J. C., & Zoback, M. D. (2000). Structure-related and stress-induced shear-wave velocity anisotropy: Observations from microearthquakes near the Calaveras Fault in Central California. *Bulletin of the Seismological Society of America*, *90*(5), 1305–1312. https://doi.org/10.1785/0119990099